

Prediction of 5-year Progression-Free Survival in Advanced Nasopharyngeal Carcinoma with Pretreatment PET/CT using Multi-Modality Deep Learning-based Radiomics

Bingxin Gu^{a,‡}, Mingyuan Meng^{b,‡}, Lei Bi^b, Jinman Kim^b, David Dagan Feng^b, Shaoli Song^{a,*}

^a Department of Nuclear Medicine, Fudan University Shanghai Cancer Center; Department of Oncology, Shanghai Medical College, Fudan University; Center for Biomedical Imaging, Fudan University; Shanghai Engineering Research Center of Molecular Imaging Probes; Key Laboratory of Nuclear Physics and Ion-beam Application (MOE), Fudan University; Shanghai, PR China.

^b School of Computer Science, the University of Sydney, Sydney, Australia.

[‡] indicates equal contribution, and * indicates corresponding author.

Abstract

Survival prediction is an important concern as it provides early prognostic information that is needed to guide the therapeutic regimen for patients with Nasopharyngeal Carcinoma (NPC). Radiomics, as a widely recognized computational method for prognosis, exploits quantitative features extracted from medical images to represent tumor characteristics that are not apparent with mere visual examination. Recently, deep learning, that leverages deep neural networks to learn deep representations (features) of patterns within images, has achieved great success on medical image analysis. Deep Learning-based Radiomics (DLR) has been considered as a replacement to the Conventional Radiomics (CR) that is dependent on handcrafted features. In this study, we aim to explore the capability of DLR for survival prediction in NPC. We developed an end-to-end multi-modality DLR model using pretreatment PET/CT images to predict 5-year Progression-Free Survival (PFS) in advanced NPC. A total of 170 patients with pathological confirmed advanced NPC (TNM stage III or IVa) were enrolled in this study. A 3D Convolutional Neural Network (CNN), with two branches to process PET and CT separately, was optimized to extract deep features from pretreatment multi-modality PET/CT images and use the derived features to predict the probability of 5-year PFS. Optionally, TNM stage, as a high-level clinical feature, can be integrated into our DLR model to further improve prognostic performance. For a comparison between CR and DLR, 1456 handcrafted features were extracted, and three top CR methods, Random Forest (RF) + RF (AUC = 0.796 ± 0.009 , testing error = 0.267 ± 0.007), RF + Adaptive Boosting (AdaBoost) (AUC = 0.783 ± 0.011 , testing error = 0.286 ± 0.009), and L^1 -Logistic Regression (L^1 -LOG) + Kernel Support Vector Machines (KSVM) (AUC = 0.769 ± 0.008 , testing error = 0.298 ± 0.006), were selected as benchmarks from 54 combinations of 6 feature selection methods and 9 classification methods. Compared to the three CR methods, our multi-modality DLR models using both PET and CT, with or without TNM stage (named PCT or PC model), resulted in the highest prognostic performance (PCT model: AUC = 0.842 ± 0.034 , testing error = 0.194 ± 0.029 ; PC model: AUC = 0.825 ± 0.041 , testing error = 0.223 ± 0.035). Furthermore, the multi-modality PCT model outperformed single-modality DLR models using only PET and TNM stage (named PT model: AUC = 0.818 ± 0.029 , testing error = 0.218 ± 0.024) or only CT and TNM stage (named CT model: AUC = 0.657 ± 0.055 , testing error = 0.375 ± 0.048). Our study identified potential radiomics-based prognostic model for survival prediction in advanced NPC, and suggests that DLR could serve as a tool for aiding in cancer management.

Keywords: Radiomics; Deep learning; Nasopharyngeal carcinoma; PET/CT

Preprint under review

1 Introduction

Nasopharyngeal Carcinoma (NPC) is a worldwide malignant epithelial cancer. The GLOBOCAN 2020 estimates that there are approximately 133,354 new NPC cases and 80,008 NPC-related deaths worldwide in 2020 (according to the International Agency for Research on Cancer (IARC)) [1]. NPC mainly arises from the nasopharynx epithelium, especially the fossa of Rosenmuller [2], and can be pathologically divided into keratinizing differentiated tumor, non-keratinizing differentiated tumor, and non-keratinizing undifferentiated tumor. Due to its unique anatomical structure and radiosensitivity [3, 4], the primary therapeutic regimen for NPC is radiotherapy (RT), with or without chemotherapy, targeted therapy, and immunotherapy. Survival prediction is a major concern in clinical cancer research, including the NPC, as it provides early prognostic information that is needed to guide the therapeutic regimen. In clinical practice, the Tumor, Node, Metastasis (TNM) stage is widely used as an indicator for survival prediction according to the American Joint Committee on Cancer (AJCC)/Union for International Cancer Control (UICC) staging system. However, for patients classified into the same TNM stage, their prognoses may differ widely and their 5-year survival rates range from 10% to 40% for advanced NPC [5-7]. This may be attributed to the fact that TNM stage only takes into account of the anatomical information, e.g., size, number, border, and location. Therefore, TNM stage can provide limited benefit for prognoses in patients with advanced NPC.

In addition to TNM stage, many clinical biomarkers, such as age, serum lactate dehydrogenase (LDH), and body mass index (BMI), have also been reported as individual prognostic indicators for survival prediction in advanced NPC [8-10]. However, these indicators are not specifically relevant to the disease and can be influenced by other indicators, thus failing in repeatability and practicability [11, 12]. Non-invasive image-derived biomarkers have also shown good prognostic performance for survival prediction in advanced NPC [13-15]. However, conventional imaging modalities, such as with Computed Tomography (CT) and Magnetic Resonance Imaging (MRI), only provide tumor's anatomical information. Multi-modality imaging of Positron Emission Tomography/Computed Tomography (PET /CT) provides both the tumor's anatomical (from CT) and metabolic (from PET) information. However, conventional indicators derived from PET/CT, including Standardized uptake Value (SUV), Metabolic Tumor Volume (MTV), and Total Lesion Glycolysis (TLG), failed to represent intra-tumor information such as tumor texture, intensity, heterogeneity, and morphology [13, 14, 16, 17]. Therefore, prognostic indicators better representing tumor characteristics, especially intra-tumor information, are in need for more accurate survival prediction.

Radiomics, as a widely recognized computational method for prognosis, exploits quantitative features (indicators) extracted from medical images to represent tumor characteristics [18]. It has drawn much attention among clinical oncologists due to its ability to provide comprehensive representations of tumor characteristics, including intra-tumor information [19]. Conventional Radiomics (CR) refers to the extraction and analysis of high-dimensional handcrafted features from medical images. Through high-throughput feature extraction and statistical machine-learning methods, CR can extract and analyze tumor characteristics and has been widely used in many clinical applications [19]. In an early study, Zhang et al. [20] performed CR-based prediction of local failure and distant failure in advanced NPC from MRI images. They experimented with 54 cross-combinations derived from 6 feature selection methods and 9 classification methods, and identified optimal combinations in terms of Area Under the receiver-operating characteristic Curve (AUC) and testing errors. In a later study, Du et al. [21] used a similar analytic scheme to identify the optimal CR methods for deafferenting local recurrence versus inflammation in NPC from PET/CT images. CR has also been studied in other cancers, such as head and

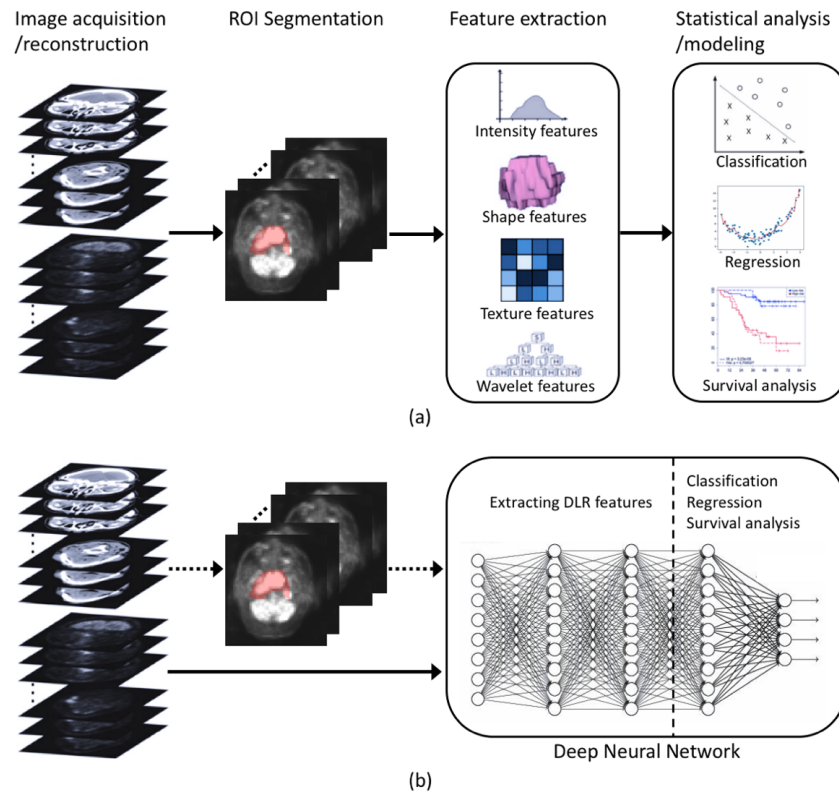


Fig.1. An illustration of radiomics process. (a) CR consisting of 4 steps: image acquisition/reconstruction, ROI segmentation, feature extraction, and statistical analysis/modeling. (b) DLR: its feature extraction and analysis are partially or fully coupled using a deep neural network. The dotted arrow indicates the optional ROI segmentation operation.

neck cancer [22] and lung cancer [23]. These studies demonstrated the capabilities of CR for prognosis and identified the optimal CR methods for their clinical targets through comprehensive comparisons. However, since CR is heavily dependent on human prior knowledge, such as handcrafted feature extraction and manual tuning of many model parameters, its limitations in bringing a source of human bias and lacking the ability to understand high-level semantic information have been well recognized [24, 25].

Recently, deep learning, that leverages deep neural networks to learn deep representations (features) of patterns within images, has achieved great success on medical image analysis and inspired trends toward Deep Learning-based Radiomics (DLR) [26]. Unlike CR normally consisting of 4 separate steps (Fig. 1a), DLR removes the reliance on using segmented Regions of Interest (ROIs), and their feature extraction and analysis are partially or fully coupled (Fig. 1b). DLR usually adopts a deep neural network to directly predict patients' outcomes from medical images in an end-to-end manner, thereby removing the reliance on time-consuming handcrafted feature extraction and allowing for automatic learning of relevant and robust features without the need for human intervention [24]. In other words, DLR can remove the human bias brought by handcrafted features and potentially discover high-level semantic features that may be overlooked by manually-defined features.

DLR has been widely used in the studies of many cancers including glioma [27], lung cancer [28], breast cancer [29], renal tumor [30], and NPC [31-34]. Peng et al. [31] proposed one of the earliest studies where DLR was introduced into the prognosis of NPC. They used a pre-trained 2D Convolutional Neural Network (CNN) to extract deep features from PET and CT images separately, and then fed the deep

features, as well as conventional handcrafted features, into a Cox Proportional Hazards (CPH) model to establish a prognostic nomogram. Their study suggested that deep features can serve as reliable and powerful indicators for prognosis. However, their 2D CNN extracted deep features from only one single tumor slice instead of the entire tumor volume, and therefore discarded important information residing in the entire tumor e.g., volumetric information [26]. Besides, their CNN was only used to extract deep features rather than to make predictions directly. This also undermines the advantages of DLR because end-to-end DLR models are considered more effective to extract relevant features [34]. In later studies, Zhang et al. [33] and Jing et al. [34] implemented end-to-end DLR models to predict the metastasis and progression of NPC from MRI images. Zhang et al. [33] still relied on a 2D CNN that takes into account of at most three tumor slices, while Jing et al. [34] used a 3D CNN to make prediction based on the entire tumor volume. Zhang et al. [33]’s and Jing et al. [34]’s DLR models both achieved higher prognostic accuracy than CR methods, they, however, only used single-modality MRI images. Existing studies have demonstrated that anatomical CT or MRI-based radiomics [22, 34, 35] showed relatively lower prognostic performance than multi-modality PET/CT-based radiomics [31, 36]. These studies suggested that PET/CT images containing both anatomical and metabolic information may be more promising for achieving higher prognostic performance. However, from our review, there is no study that attempted to develop end-to-end DLR models for predicting the prognoses of NPC patients from PET/CT images. In addition, existing DLR studies [27-30, 32-34] are further limited by: (1) they were mainly designed for single imaging modality such as MRI and CT, so their DLR models cannot derive complementary features from multi-modality PET/CT images; and (2) they had limited comparison to the CR methods (e.g., only a few CR methods were chosen for comparison), which undermines the reliability of their conclusions.

In this study, we investigated DLR for long-time (5-year) survival prediction in 170 patients with advanced NPC using pretreatment PET/CT images. We employed an end-to-end multi-modality DLR model to directly predict 5-year Progression-Free Survival (PFS) from pretreatment PET/CT images. Our DLR model is a 3D CNN that was purposely optimized for multi-modality PET/CT images and can simultaneously extract complementary deep features from both PET and CT images. Our DLR model can integrate TNM stage as a high-level clinical feature and this has been demonstrated to further improve prognostic performance. In the experiments, we first followed the analytic scheme proposed by Zhang et al. [20] to identify the optimal CR methods as benchmarks, and then compared our DLR model with these benchmarks for prognostic performance. Furthermore, we also established single-modality DLR models using only PET or CT for comparison. Our results demonstrated that DLR can outperform CR in survival prediction of NPC, and that the multi-modality DLR model can achieve higher prognostic performance than the single-modality DLR models.

2 Material and methods

2.1 Patients and PET/CT image data

From November 2009 to March 2014, a total of 170 patients pathologically confirmed with advanced NPC (TNM stage III or IVa) were retrospectively enrolled in this study. All patients received therapeutic regimen at Fudan University Shanghai Cancer Center (FUSCC) according to the NCCN guidelines. Treatment responses were identified by imaging examination according to RECIST 1.1 [37]. The following endpoint was set as PFS or follow-up date of more than 5 years. PFS was defined as the time from the first day of treatment to the day of disease progression or otherwise censored. FUSCC Ethical Committee approved this study, and informed consent was obtained from all enrolled patients.

All patients underwent ^{18}F -fluorodeoxyglucose (FDG) PET/CT (Siemens Biograph 16HR, Knoxville, Tennessee, USA) prior to treatment within 4 weeks. ^{18}F -FDG was produced automatically by cyclotron (Siemens CTI RDS Eclips ST, Knoxville, Tennessee, USA) using Explora FDG₄ module in our center. The radiochemical purity of ^{18}F -FDG was over 95%. Patients were requested to fast 4-6 h to maintain the venous blood glucose levels under 10 mmol/L before scanning. Each patient got injected with 7.4 MBq/kg ^{18}F -FDG, then kept lying comfortably in a quiet, dimly lit room for approximately 1 h prior to scanning. Images were obtained on a Siemens biograph 16HR PET/CT scanner (Knoxville, Tennessee, USA). Data acquisition procedure was as follows: CT scanning was first performed, from the proximal thighs to head, with 120 kV, 80 ~ 250 mA, pitch 3.6, rotation time 0.5. Immediately after CT scanning, a PET emission scan that covered the identical transverse field of view was obtained. Acquisition time was 2 ~ 3 min per table position. PET images were reconstructed iteratively using an ordered-subset expectation maximization iterative reconstruction (OSEM) by applying CT images for attenuation correction.

2.2 Problem definition

We aimed for long-time survival prediction in patients with advanced NPC using pretreatment PET/CT images. In this study, we mainly focused on 5-year PFS and regarded the survival prediction as a binary classification problem. Specifically, patients who experienced a relapse after treatment within the 5 years were labeled as 1, while other patients were labeled as 0. Then, the objective of this study was to classify patients into these two labeled classes using pretreatment PET/CT images. TNM stage, as supplementary information, is optional for this problem to further improve prognostic performance.

2.3 Data preprocessing

Before PET/CT images were fed into the CR workflow or into our DLR models, they were preprocessed through the following steps: (1) Primary tumors were segmented on PET and CT images simultaneously using a semi-automatic segmentation algorithm on ITK-SNAP software [38], and followed by manual adjustment to ensure reliability. This process was performed by two experienced nuclear medicine physicians independently, and they reached a consensus in case of inconsistency. (2) PET images were normalized based on body mass. The derived body mass was applied to convert PET images into SUV maps. (3) PET/CT images and tumor segmentation masks were resampled into isotropic voxels of unit dimension to ensure comparability, where 1 voxel corresponds to 1 mm³. Specifically, PET/CT images and segmentation masks were resampled via linear interpolation and nearest neighbor interpolation, respectively. (4) PET/CT images were multiplied with the binary masks of tumor segmentations to extract ROI, and then were cropped into three-dimensional patches with a size of 80×80×64 voxels. The patch size was selected to ensure that the whole segmented tumor can be included and the tumor center aligned with the patch center. (5) The patches were then normalized to a 0-1 range using 95% of maximal and minimal pixel values as upper and lower limits. The pixels whose values are higher/lower than upper/lower limit were cut off to be 1/0.

We randomly divided all 170 patients into a training cohort (120 patients) and an external validation cohort (50 patients). To reduce the sampling bias led by cohort division, all experiments were repeatedly carried out for 10 times. In all repeated experiments, all patients were randomly re-divided into a new training cohort and a new external validation cohort. Finally, the average results over all the repetitions were calculated.

2.4 Conventional radiomics (CR) analysis

For performing a comprehensive comparison between DLR and CR, we first followed the analytic scheme proposed by Zhang et al. [20] to identify the optimal CR methods for our research objective, and then the optimal methods were chosen as benchmarks and compared to our DLR model in the following analysis. Concretely, we experimented with 54 cross-combinations derived from 6 feature selection methods and 9 classification methods, and then identified the top-3 optimal combinations in terms of both AUC and testing error. The 6 feature selection methods and 9 classification methods used in the analysis are listed in Table I.

We extracted handcrafted radiomics features from the preprocessed PET/CT patches for each patient, including 19 features from First Order Statistics (FOS), 24 features from Grey-Level Cooccurrence Matrix (GLCM), 16 features from Grey-Level Run Length Matrix (GLRLM), 16 features from Grey-Level Size Zone Matrix (GLSZM), 5 features from Neighboring Grey Tone Difference Matrix (NGTDM), and 16 features based on 3D shape of tumor. FOS and textural features (i.e., GLCM, GLRLM, GLSZM, and NGTDM) were also recomputed after different wavelet decomposition in three directions (x, y, z) of the original images. Performing low-pass or high-pass wavelet filter along x, y, or z directions resulted in 8 decompositions of original image. Consequently, we extracted a total of 1456 features. All feature extraction was implemented using Pyradiomics [39], an open-source python package for the extraction of radiomics features from medical images. Besides, we also regarded TNM stage as a clinical feature because it showed high relevance to PFS in our previous study [11].

The radiomics features were first fed into a feature selection model to screen the most robust and relevant features. Then, both the selected radiomics features and clinical feature (i.e., TNM stage) were fed into a classification model for statistical analysis. Note that all models were trained only using the training cohort, and their prognostic performance was evaluated in the external validation cohort. All hyper-parameters were chosen through cross-validation in the training cohort, and the number of the selected radiomics features was also regarded as a hyper-parameter. All analyses were performed using R packages (version 3.6.3, <http://www.R-project.org>).

Table I. The feature selection methods and classification methods used in the CR analysis.

Category	Name (Acronym)
Feature selection methods	L ¹ -Logistic Regression (L ¹ -LOG) L ¹ -Support Vector Machine (L ¹ -SVM) Random Forest (RF) Distance Correlation (DC) Elastic Net Logistic Regression (EN-LOG) Sure Independence Screening (SIS)
Classification methods	L ² -Logistic Regression (L ² -LOG) Kernel Support Vector Machines (KSVM) Linear-SVM (LSVM) Adaptive Boosting (AdaBoost) Random Forest (RF) Neural Network (Nnet) K-nearest neighborhood (KNN) Linear Discriminant Analysis (LDA) Naive Bayes (NB)

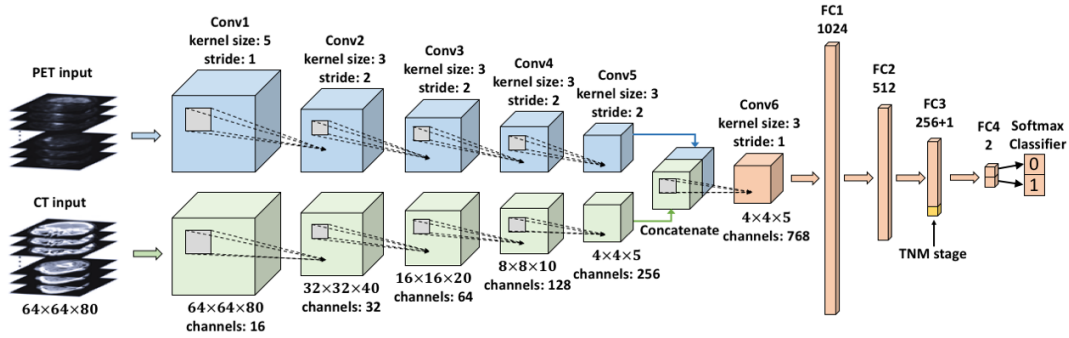


Fig.2. An illustration of the deep neural network used in the DLR analysis. This network takes a pair of PET/CT images and a clinical feature (i.e., TNM stage) as input, and the final layer (FC4) outputs normalized probabilities for both classes (0 = alive, 1 = relapse).

2.5 Deep learning-based radiomics (DLR) analysis

We employed an end-to-end multi-modality DLR model to directly predict patients' 5-year PFS from pretreatment PET/CT images. This DLR model is a 3D CNN and its architecture is based on 3DMCL [25], a deep multi-modality architecture for predicting the distant metastases of soft-tissue sarcoma from PET/CT images. The architecture of our DLR model is shown in Fig.2. In this architecture, there are two separate branches processing the PET and CT images in a simultaneous manner. For each PET and CT branch, there are five convolutional layers (Conv1-5) of 16, 32, 64, 128, and 256 filters with kernel sizes of 5, 3, 3, 3, and 3, respectively. The middle four convolutional layers (Conv2-5) are with a stride of 2 to reduce the resolution of feature maps. To fuse the feature maps derived from both branches, the output of PET and CT branches are concatenated together, and then are fed into another convolutional layer (Conv6) of 768 filters with kernel size of 3. Each convolutional layer is followed by a batch normalization layer and an ELU activation. The feature maps obtained from the last convolutional layer (Conv6) are considered as deep features with high-level semantic information related to tumor characteristics. Finally, four fully-connected layers (FC1-4), which have 1024, 512, 256 and 2 nodes respectively, are added to perform survival prediction based on deep features. The first three fully-connected layers (FC1-3) are followed by a ReLU activation and a dropout layer, while the last layer (FC4) is followed by a softmax classifier layer which outputs normalized probabilities of two classes (0 = alive, 1 = relapse). Besides, TNM stage, as a high-level clinical feature, can be concatenated with the third fully-connected layer (FC3).

In addition to the above DLR model that took all PET, CT, and TNM stage as input (named PCT model), we also established three DLR models to evaluate the values of PET/CT images and TNM stage for survival prediction: (1) PC model: a DLR model that took PET and CT images as input. In this model, TNM stage was not concatenated with FC3. (2) PT model: a DLR model that took PET images and TNM stage as input. In this model, CT branch was truncated and only PET branch was connected to Conv6. (3) CT model: a DLR model that took CT images and TNM stage as input. In this model, PET branch was truncated and only CT branch was connected to Conv6.

All DLR models were implemented using Keras with a Tensorflow backend on a 12GB TITAN V GPU. We used the Adam optimizer with a batch size of 32 and learning rate of 0.0001 for training the model. Cross-entropy loss function was used as the loss and our training stops when there are no further drops on the total loss. The models were trained with the training cohort. All the hyper-parameters, including batch size, learning rate, dropout rate, and regularization terms, were chosen through cross-

validation in the training cohort. Since we only have a relatively small dataset, during the training stage, data augmentation was applied to the patches in real time to avoid overfitting. The used data augmentation techniques included random translations ± 8 pixels in all 3 axes, random rotation along the longitudinal axes, and random flipping along all 3 axes.

3 Results

3.1 Patients

A total of 170 advanced NPC patients (female = 40, male = 130; median age = 46, range 16-78; TNM stage III = 121, TNM stage IVa = 49) were included in this study. With more than 5 years follow up, 48 out of 170 (28.24%) patients suffered a relapse after treatment within the first 5 years.

3.2 Prognostic performance of conventional radiomics (CR)

AUC and testing error were applied to quantify the prognostic performance of different cross-combinations of feature selection and classification methods. A total of 54 cross-combinations were generated from 6 feature selection methods and 9 classification methods. As shown in Fig. 3, the top five mean AUC of cross-combinations are RF + RF (0.796 ± 0.009 , range 0.752-0.833), RF + AdaBoost (0.783 ± 0.011 , range 0.744-0.827), SIS + LSVM (0.778 ± 0.014 , range 0.731-0.824), L¹-LOG + L²-LOG (0.772 ± 0.007 , range 0.745-0.806), and L¹-LOG + KSVM (0.769 ± 0.008 , range 0.735-0.808). As demonstrated in Fig.4, the bottom five mean testing error of cross-combinations are RF + RF (0.267 ± 0.007 , range 0.234-0.301), RF + KSVM (0.283 ± 0.007 , range 0.247-0.318), RF + AdaBoost (0.286 ± 0.009 , range 0.244-0.321), L¹-LOG + KSVM (0.298 ± 0.006 , range 0.262-0.327), and RF + KNN (0.301 ± 0.008 , range 0.260-0.338).

Scatterplot was used to screen out the cross-combinations with high AUC and low testing error. Fig. 5 illustrates that the optimal cross-combinations are RF + RF (AUC = 0.796 ± 0.009 , testing error = 0.267 ± 0.007), RF + AdaBoost (AUC = 0.783 ± 0.011 , testing error = 0.286 ± 0.009), and L¹-LOG + KSVM (AUC = 0.769 ± 0.008 , testing error = 0.298 ± 0.006), which show higher prognostic performance than the other cross-combinations.

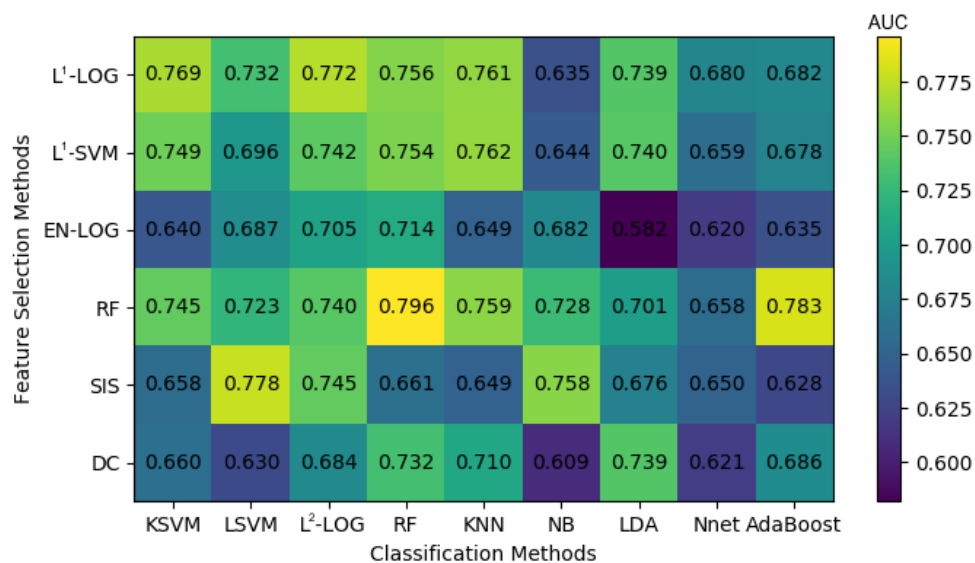


Fig. 3. A heatmap depicting the average AUC of all cross-combinations derived from 6 feature selection methods (in rows) and 9 classification methods (in columns).

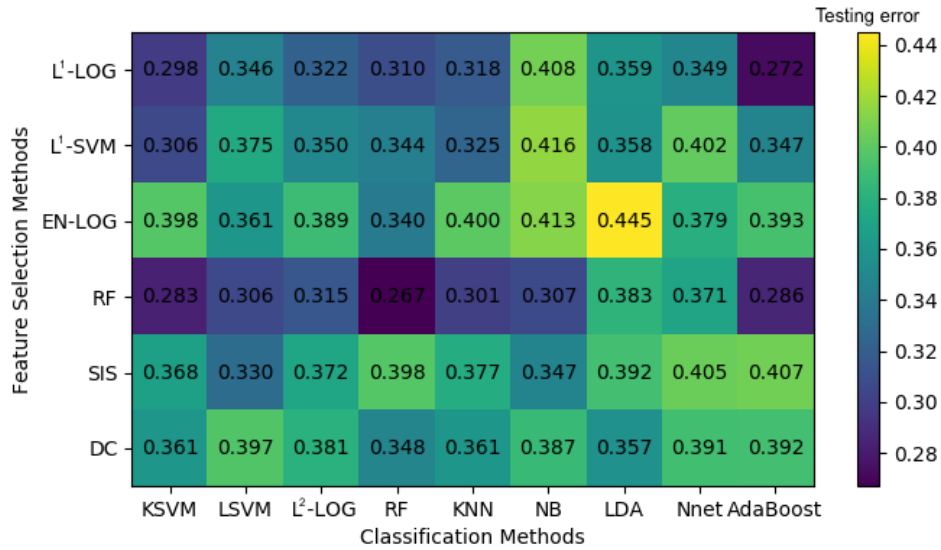


Fig. 4. A heatmap depicting the average testing error of all cross-combinations derived from 6 feature

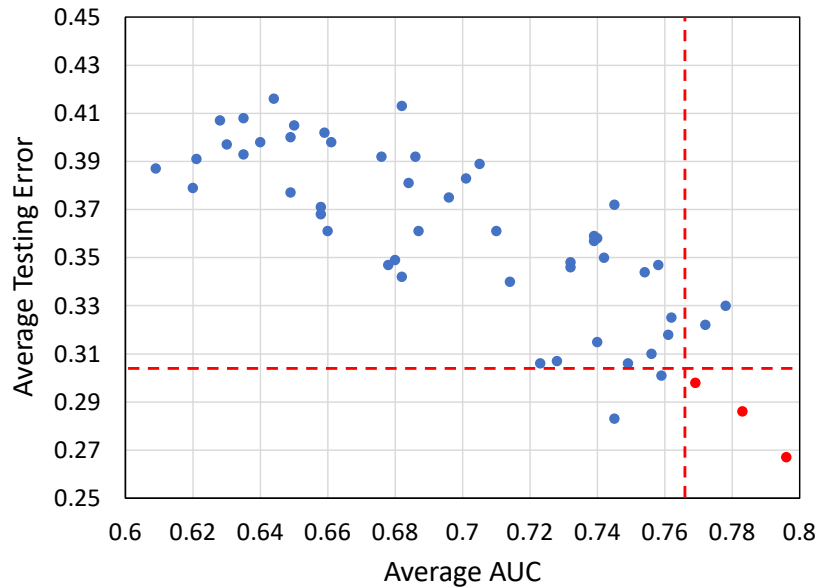


Fig. 5. A scatterplot depicting the average AUC and testing error of all 54 cross-combinations derived from 6 feature selection methods and 9 classification methods. Two red dotted lines distinguish the combinations that show top-5 performance in AUC and in testing error. Three highly reliable and prognostic combinations that show top-5 performance in both AUC and testing error (RF + RF, RF + AdaBoost, and L1-LOG + KSVM) are displayed in red points.

3.3 Prognostic performance of deep learning-based radiomics (DLR)

As shown in Fig. 6, the PCT model has the highest prognostic performance (AUC = 0.842 ± 0.034 ; range, 0.778-0.912), while PC model and PT model show lower but also good prognostic performance (AUC = 0.825 ± 0.041 ; range, 0.752-0.887; AUC = 0.818 ± 0.029 ; range, 0.754-0.873; respectively). However, CT model shows much lower prognostic performance (AUC = 0.657 ± 0.055 ; range, 0.564-0.728). Furthermore, PCT model also shows higher performance in testing error, recall, and F1 score (Table II).

Table II. Comparison among three DLR models.

Method	AUC	Testing error	Precision	Recall	F1 score
PCT model (PET + CT + TNM stage)	0.842 (0.034) [0.778, 0.912]	0.194 (0.029) [0.132, 0.258]	0.725 (0.046) [0.642, 0.811]	0.853 (0.053) [0.744, 0.947]	0.784 (0.027) [0.719, 0.858]
PC model (PET + CT)	0.825 (0.041) [0.752, 0.887]	0.223 (0.035) [0.163, 0.287]	0.712 (0.042) [0.636, 0.798]	0.795 (0.049) [0.697, 0.894]	0.751 (0.019) [0.712, 0.796]
PT model (PET + TNM stage)	0.818 (0.029) [0.754, 0.873]	0.218 (0.024) [0.164, 0.268]	0.786 (0.038) [0.709, 0.832]	0.707 (0.042) [0.623, 0.788]	0.744 (0.027) [0.693, 0.804]
CT model (CT + TNM stage)	0.657 (0.055) [0.564, 0.728]	0.375 (0.048) [0.297, 0.442]	0.512 (0.083) [0.417, 0.594]	0.668 (0.075) [0.568, 0.758]	0.579 (0.064) [0.492, 0.662]

Note: The average results are reported with standard deviation in the parenthesis, 0.25 and 0.75th quantile values in the bracket. The highest result in each column is in bold.

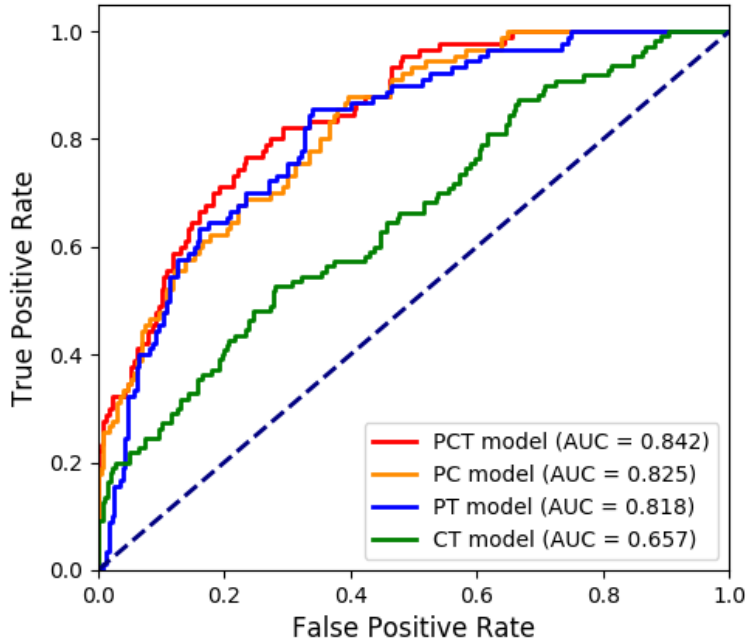


Fig. 6. Comparison among three DLR models through ROC curve.

3.4 Comparison between DLR and CR

We further compared our multi-modality DLR model (PCT model) with the identified optimal CR methods (RF + RF, RF + AdaBoost, and L^1 -LOG + KSVM). Fig. 7 demonstrates that our DLR model has the highest prognostic performance compared with the three CR methods. Furthermore, our DLR model has the lowest testing error, highest precision, recall, and F1 score among these methods (Table III). Therefore, our multi-modality PET/CT-derived DLR model could better predict the 5-year PFS in advanced NPC patients.

Table III. Comparison among the optimal conventional radiomics methods and DLR model.

Method	AUC	Testing error	Precision	Recall	F1 score
L ¹ -LOG + KSVM	0.769 (0.008) [0.735, 0.808]	0.298 (0.006) [0.262, 0.327]	0.688 (0.017) [0.624, 0.741]	0.752 (0.013) [0.706, 0.803]	0.719 (0.009) [0.678, 0.757]
RF + AdaBoost	0.783 (0.011) [0.744, 0.827]	0.286 (0.009) [0.244, 0.321]	0.668 (0.014) [0.614, 0.717]	0.814 (0.019) [0.756, 0.873]	0.734 (0.012) [0.693, 0.775]
RF + RF	0.796 (0.009) [0.752, 0.833]	0.267 (0.007) [0.234, 0.301]	0.712 (0.010) [0.669, 0.758]	0.734 (0.012) [0.691, 0.773]	0.723 (0.008) [0.685, 0.763]
DLR (PCT model)	0.842 (0.034) [0.778, 0.912]	0.194 (0.029) [0.132, 0.258]	0.725 (0.046) [0.642, 0.811]	0.853 (0.053) [0.744, 0.947]	0.784 (0.027) [0.719, 0.858]

Note: The average results are reported with standard deviation in the parenthesis, 0.25 and 0.75th quantile values in the bracket. The highest result in each column is in bold.

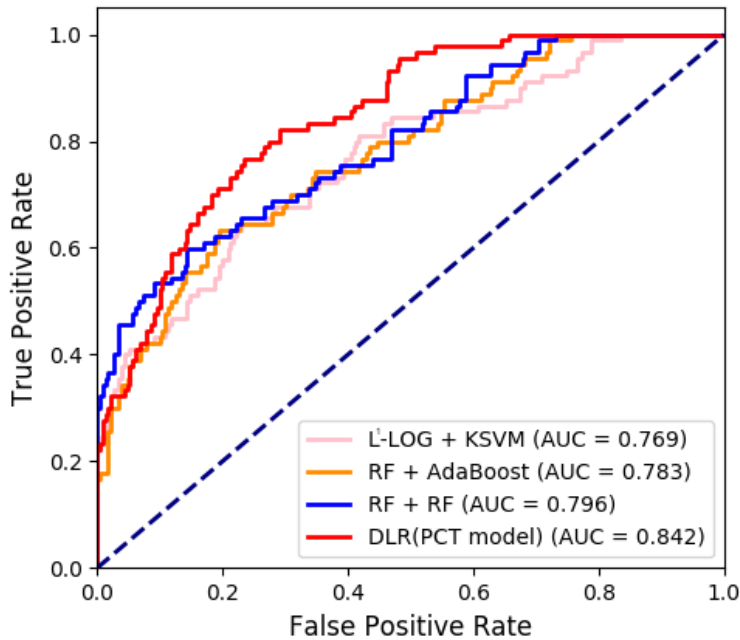


Fig. 7. Comparison among the optimal CR methods and DLR model through ROC curve.

4 Discussion

Pretreatment medical images contain much more information than diagnosis and TNM stage. However, clinical oncologists usually only employ “visible” information in routine clinical practice and in treatment planning. Radiomics employs a large amount of tumor information, especially intra-tumor information, which can be used for aiding in prognostic prediction [22, 23, 40]. CR depends heavily on handcrafted feature extraction and manual tuning of statistical models. Therefore, in some studies [20-23, 35], different feature extraction schemes, feature selection methods, and statistical models were investigated to identify optimal CR methods for a specific clinical target. Our study was motivated by the analytic scheme proposed by Zhang et al. [20], and we derived 54 cross-combinations from 6 feature selection methods and 9 classification methods. Considering both AUC and testing error (Fig. 5), the optimal combinations was RF + RF and RF +

AdaBoost, which is consistent with Zhang et al.'s study [20]. However, it should be noted that the AUC of RF + RF and RF + AdaBoost were 0.796 ± 0.009 and 0.783 ± 0.011 , which are lower than Zhang et al.'s results [20] ($AUC = 0.8464 \pm 0.0069$ and 0.8204 ± 0.0095 , respectively). This is likely due to the different clinical targets and different follow-up durations. We focused on the prediction of long-time (5-year) PFS in advanced NPC, while Zhang et al. [20] focused on the prediction of local/distant failure and didn't clearly point out their follow-up duration.

DLR is considered as a replacement for CR and has demonstrated superior prognostic performance in some studies [20]. However, there are only few studies where DLR was comprehensively compared with CR. In most case [27-30, 32-34], only a few CR methods were chosen as the benchmarks, but there is no guarantee that the chosen methods are optimal for their clinical targets. In our study, we first evaluated 54 CR combinations, and then the three optimal combinations (RF + RF, RF + AdaBoost and L^1 -LOG + KSVM) were chosen as the benchmarks for further comparison with our DLR model. Our DLR models showed the greatest performance in prognosis (Fig. 7 and Table III). Through comprehensive comparison, we suggest that DLR is superior than CR in the prediction of long-time PFS in advanced NPC. We attribute this superiority to three main reasons: First, DLR allows for automatic learning of robust and relevant features from multi-modality PET/CT images, which reduces the human bias (or even errors) caused by handcrafted feature extraction. Second, the automatic feature learning possibly could discover some high-level semantic features that may be overlooked by manually-defined feature extraction. Third, it has been widely recognized that CNNs have outstanding ability for pattern recognition [20], so DLR can inherit this ability by employing CNN architectures.

Although DLR has been applied for prognosis of NPC in several previous studies [31, 33, 34], there still exist following limitations: Peng et al. [31] only used a 2D CNN to extract deep features rather than to directly predict survival outcomes in an end-to-end manner, and the deep features were extracted from only one single tumor slice instead of the entire tumor volume. Jing et al. [34] overcame the aforementioned limitations by employing a 3D end-to-end DLR model that directly predicts the risk of disease progression based on the entire tumor volume. Their study demonstrated that end-to-end DLR models are more effective to extract relevant features and showed higher prognostic performance, but their study was limited by using single-modality MRI. Zhang et al. [33] also used an end-to-end DLR model to directly predict Distant Metastasis-Free Survival (DMFS), but their study suffered from the same limitations as Peng et al. [31]'s and Jing et al. [34]'s ones: they also used a 2D CNN that makes decision based on at most three tumor slices, and their study was also limited by using single-modality MRI. In this study, we have overcome these limitations by developing a 3D multi-modality end-to-end DLR model that was purposely optimized for PET/CT images. In contrast to Peng et al. [31]'s study where deep features were separately extracted from PET and CT images, our DLR model can simultaneously extract complementary deep features from both PET and CT images. In the experiments, since Zhang et al. [33]'s and our studies both focused on similar clinical targets (DMFS and PSF) and used the same evaluation metrics (AUC), their result can be directly compared with ours. Our multi-modality DLR model (PCT model) showed higher prognostic performance than Zhang et al. [33]'s method (AUC of 0.842 versus 0.796), in spite of the fact that Zhang et al. [33] employed additional information (e.g., plasma Epstein-Barr virus (EBV) DNA and treatment regimens) for prediction. The result demonstrates that, by overcoming the aforementioned limitations with a 3D PET/CT-based end-to-end DLR model, our study indeed gained improvements over previous DLR studies in NPC.

We compared our multi-modality DLR model (PCT model) with two single-modality DLR models (PT and CT model) for additional comparisons. The results showed that the PCT model outperformed the PT and CT models (Fig. 6 and Table II), which suggests that integrating both metabolic (from PET) and anatomical (from CT) information is helpful for achieving higher prognostic performance. It also should be noted that the CT model showed much lower prognostic performance than the PCT and PT model. This suggests that metabolic information may be more crucial for survival prediction in NPC. This is possibly because metabolic information could reflect intra-tumor heterogeneity [41]. Nevertheless, anatomical information can still facilitate survival prediction when integrated with metabolic information.

TNM stage, as a high-level clinical feature, is optionally used in our DLR models (PCT, PT, and CT models) to further improve the prognostic performance. For evaluating the value of TNM stage, we established a DLR model excluding TNM stage (PC model). The results showed that the PC model has degraded prognostic performance compared to the PCT model (Fig. 6 and Table II), which suggests that TNM stage can provide supplementary information and enhance the prognostic performance of survival prediction in NPC patients. Nevertheless, it should be noted that the three optimal CR methods also used TNM stage, but they still showed lower prognostic performance than the PC model, which suggested that TNM stage is useful but not crucial for the survival prediction.

5 Conclusion

We introduced and evaluated an end-to-end multi-modality DLR model in predicting 5-year PFS of patients with advanced NPC using pretreatment PET/CT images. Our results demonstrated that our multi-modality DLR models improved prognostic performance over CR methods. Furthermore, our multi-modality DLR models outperformed single-modality DLR models. Our study suggested that multi-modality DLR derived from pretreatment PET/CT could serve as a potential tool for aiding in cancer management.

Reference

- [1] H. Sung, J. Ferlay, R.L. Siegel, M. Laversanne, I. Soerjomataram, A. Jemal, F. Bray, Global cancer statistics 2020: GLOBOCAN estimates of incidence and mortality worldwide for 36 cancers in 185 countries, *CA Cancer J Clin*, (2021).
- [2] M.L.K. Chua, J.T.S. Wee, E.P. Hui, A.T.C. Chan, Nasopharyngeal carcinoma, *The Lancet*, 387 (2016) 1012-1024.
- [3] L. Ribassin-Majed, S. Marguet, A.W.M. Lee, W.T. Ng, J. Ma, A.T.C. Chan, P.Y. Huang, G. Zhu, D.T.T. Chua, Y. Chen, H.Q. Mai, D.L.W. Kwong, S.L. Cheah, J. Moon, Y. Tung, K.H. Chi, G. Fountzilias, J. Bourhis, J.P. Pignon, P. Blanchard, What Is the Best Treatment of Locally Advanced Nasopharyngeal Carcinoma? An Individual Patient Data Network Meta-Analysis, *Journal of clinical oncology : official journal of the American Society of Clinical Oncology*, 35 (2017) 498-505.
- [4] A.W. Lee, B.B. Ma, W.T. Ng, A.T. Chan, Management of Nasopharyngeal Carcinoma: Current Practice and Future Perspective, *Journal of clinical oncology : official journal of the American Society of Clinical Oncology*, 33 (2015) 3356-3364.
- [5] C.I. Huang, L.F. Chen, S.L. Chang, H.C. Wu, W.C. Ting, C.C. Yang, Accuracy of a Staging System for Prognosis of 5-Year Survival of Patients With Nasopharyngeal Carcinoma Who Underwent Chemoradiotherapy, *JAMA Otolaryngol Head Neck Surg*, 143 (2017) 1086-1091.

- [6] X.-R. Tang, Y.-Q. Li, S.-B. Liang, W. Jiang, F. Liu, W.-X. Ge, L.-L. Tang, Y.-P. Mao, Q.-M. He, X.-J. Yang, Y. Zhang, X. Wen, J. Zhang, Y.-Q. Wang, P.-P. Zhang, Y. Sun, J.-P. Yun, J. Zeng, L. Li, L.-Z. Liu, N. Liu, J. Ma, Development and validation of a gene expression-based signature to predict distant metastasis in locoregionally advanced nasopharyngeal carcinoma: a retrospective, multicentre, cohort study, *The Lancet Oncology*, 19 (2018) 382-393.
- [7] Y. Lei, Y.Q. Li, W. Jiang, X.H. Hong, W.X. Ge, Y. Zhang, W.H. Hu, Y.Q. Wang, Y.L. Liang, J.Y. Li, W.C.S. Cho, J.P. Yun, J. Zeng, J.W. Chen, L.Z. Liu, L. Li, L. Chen, F.Y. Xie, W.F. Li, Y.P. Mao, X. Liu, Y.P. Chen, L.L. Tang, Y. Sun, N. Liu, J. Ma, A Gene-Expression Predictor for Efficacy of Induction Chemotherapy in Locoregionally Advanced Nasopharyngeal Carcinoma, *Journal of the National Cancer Institute*, (2020).
- [8] J.K. Cho, G.J. Lee, K.I. Yi, K.S. Cho, N. Choi, J.S. Kim, H. Kim, D. Oh, S.K. Choi, S.H. Jung, H.S. Jeong, Y.C. Ahn, Development and external validation of nomograms predictive of response to radiation therapy and overall survival in nasopharyngeal cancer patients, *Eur J Cancer*, 51 (2015) 1303-1311.
- [9] L.Q. Tang, C.F. Li, J. Li, W.H. Chen, Q.Y. Chen, L.X. Yuan, X.P. Lai, Y. He, Y.X. Xu, D.P. Hu, S.H. Wen, Y.T. Peng, L. Zhang, S.S. Guo, L.T. Liu, L. Guo, Y.S. Wu, D.H. Luo, P.Y. Huang, H.Y. Mo, Y.Q. Xiang, R. Sun, M.Y. Chen, Y.J. Hua, X. Lv, L. Wang, C. Zhao, K.J. Cao, C.N. Qian, X. Guo, Y.X. Zeng, H.Q. Mai, M.S. Zeng, Establishment and Validation of Prognostic Nomograms for Endemic Nasopharyngeal Carcinoma, *Journal of the National Cancer Institute*, 108 (2016).
- [10] J. Li, S. Chen, S. Peng, Y. Liu, S. Xing, X. He, H. Chen, Prognostic nomogram for patients with Nasopharyngeal Carcinoma incorporating hematological biomarkers and clinical characteristics, *Int J Biol Sci*, 14 (2018) 549-556.
- [11] B. Gu, J. Zhang, G. Ma, S. Song, L. Shi, Y. Zhang, Z. Yang, Establishment and validation of a nomogram with intratumoral heterogeneity derived from (18)F-FDG PET/CT for predicting individual conditional risk of 5-year recurrence before initial treatment of nasopharyngeal carcinoma, *BMC Cancer*, 20 (2020) 37.
- [12] F.P. Chen, L. Lin, Z.Y. Qi, G.Q. Zhou, R. Guo, J. Hu, A.H. Lin, J. Ma, Y. Sun, Pretreatment Nomograms for Local and Regional Recurrence after Radical Radiation Therapy for Primary Nasopharyngeal Carcinoma, *J Cancer*, 8 (2017) 2595-2603.
- [13] S.C. Chan, C.L. Hsu, T.C. Yen, S.H. Ng, C.T. Liao, H.M. Wang, The role of 18F-FDG PET/CT metabolic tumour volume in predicting survival in patients with metastatic nasopharyngeal carcinoma, *Oral Oncol*, 49 (2013) 71-78.
- [14] K.P. Chang, N.M. Tsang, C.T. Liao, C.L. Hsu, M.J. Chung, C.W. Lo, S.C. Chan, S.H. Ng, H.M. Wang, T.C. Yen, Prognostic significance of 18F-FDG PET parameters and plasma Epstein-Barr virus DNA load in patients with nasopharyngeal carcinoma, *J Nucl Med*, 53 (2012) 21-28.
- [15] L. Zhang, D. Dong, H. Li, J. Tian, F. Ouyang, X. Mo, B. Zhang, X. Luo, Z. Lian, S. Pei, Y. Dong, W. Huang, C. Liang, J. Liu, S. Zhang, Development and validation of a magnetic resonance imaging-based model for the prediction of distant metastasis before initial treatment of nasopharyngeal carcinoma: A retrospective cohort study, *EBioMedicine*, 40 (2019) 327-335.
- [16] Y.H. Chen, K.P. Chang, S.C. Chu, T.C. Yen, L.Y. Wang, J.T. Chang, C.L. Hsu, S.H. Ng, S.H. Liu, S.C. Chan, Value of early evaluation of treatment response using (18)F-FDG PET/CT parameters and the Epstein-Barr virus DNA load for prediction of outcome in patients with primary nasopharyngeal carcinoma, *Eur J Nucl Med Mol Imaging*, 46 (2019) 650-660.
- [17] B. Ma, E.P. Hui, A. King, S.F. Leung, M.K. Kam, F. Mo, L. Li, K. Wang, H. Loong, A. Wong, C.M.

- Chan, K.C.A. Chan, S.C.C. Wong, Y.M.D. Lo, A.T. Chan, Prospective evaluation of plasma Epstein-Barr virus DNA clearance and fluorodeoxyglucose positron emission scan in assessing early response to chemotherapy in patients with advanced or recurrent nasopharyngeal carcinoma, *Br J Cancer*, 118 (2018) 1051-1055.
- [18] R.J. Gillies, P.E. Kinahan, H. Hricak, Radiomics: Images Are More than Pictures, They Are Data, *Radiology*, 278 (2016) 563-577.
- [19] M. Sollini, L. Antunovic, A. Chiti, M. Kirienko, Towards clinical application of image mining: a systematic review on artificial intelligence and radiomics, *Eur J Nucl Med Mol Imaging*, 46 (2019) 2656-2672.
- [20] B. Zhang, X. He, F. Ouyang, D. Gu, Y. Dong, L. Zhang, X. Mo, W. Huang, J. Tian, S. Zhang, Radiomic machine-learning classifiers for prognostic biomarkers of advanced nasopharyngeal carcinoma, *Cancer Lett*, 403 (2017) 21-27.
- [21] D. Du, H. Feng, W. Lv, S. Ashrafinia, Q. Yuan, Q. Wang, W. Yang, Q. Feng, W. Chen, A. Rahmim, L. Lu, Machine Learning Methods for Optimal Radiomics-Based Differentiation Between Recurrence and Inflammation: Application to Nasopharyngeal Carcinoma Post-therapy PET/CT Images, *Mol Imaging Biol*, 22 (2020) 730-738.
- [22] C. Parmar, P. Grossmann, D. Rietveld, M.M. Rietbergen, P. Lambin, H.J. Aerts, Radiomic Machine-Learning Classifiers for Prognostic Biomarkers of Head and Neck Cancer, *Front Oncol*, 5 (2015) 272.
- [23] Y. Zhang, A. Oikonomou, A. Wong, M.A. Haider, F. Khalvati, Radiomics-based Prognosis Analysis for Non-Small Cell Lung Cancer, *Sci Rep*, 7 (2017) 46349.
- [24] A. Hosny, H.J. Aerts, R.H. Mak, Handcrafted versus deep learning radiomics for prediction of cancer therapy response, *Lancet Digit Health*, 1 (2019) e106-e107.
- [25] Y. Peng, L. Bi, Y. Guo, D. Feng, M. Fulham, J. Kim, Deep multi-modality collaborative learning for distant metastases predication in PET-CT soft-tissue sarcoma studies, *Annu Int Conf IEEE Eng Med Biol Soc*, 2019 (2019) 3658-3688.
- [26] P. Afshar, A. Mohammadi, K.N. Plataniotis, A. Oikonomou, H. Benali, From Handcrafted to Deep-Learning-Based Cancer Radiomics: Challenges and Opportunities, *IEEE Signal Processing Magazine*, 36 (2019) 132-160.
- [27] Z. Li, Y. Wang, J. Yu, Y. Guo, W. Cao, Deep Learning based Radiomics (DLR) and its usage in noninvasive IDH1 prediction for low grade glioma, *Sci Rep*, 7 (2017) 5467.
- [28] A. Hosny, C. Parmar, T.P. Coroller, P. Grossmann, R. Zeleznik, A. Kumar, J. Bussink, R.J. Gillies, R.H. Mak, H. Aerts, Deep learning for lung cancer prognostication: A retrospective multi-cohort radiomics study, *PLoS Med*, 15 (2018) e1002711.
- [29] N. Naik, A. Madani, A. Esteva, N.S. Keskar, M.F. Press, D. Ruderman, D.B. Agus, R. Socher, Deep learning-enabled breast cancer hormonal receptor status determination from base-level H&E stains, *Nat Commun*, 11 (2020) 5727.
- [30] L. Zhou, Z. Zhang, Y.C. Chen, Z.Y. Zhao, X.D. Yin, H.B. Jiang, A Deep Learning-Based Radiomics Model for Differentiating Benign and Malignant Renal Tumors, *Transl Oncol*, 12 (2019) 292-300.
- [31] H. Peng, D. Dong, M.J. Fang, L. Li, L.L. Tang, L. Chen, W.F. Li, Y.P. Mao, W. Fan, L.Z. Liu, L. Tian, A.H. Lin, Y. Sun, J. Tian, J. Ma, Prognostic Value of Deep Learning PET/CT-Based Radiomics: Potential Role for Future Individual Induction Chemotherapy in Advanced Nasopharyngeal Carcinoma, *Clin Cancer Res*, 25 (2019) 4271-4279.
- [32] W.Y. Chuang, S.H. Chang, W.H. Yu, C.K. Yang, C.J. Yeh, S.H. Ueng, Y.J. Liu, T.D. Chen, K.H. Chen, Y.Y. Hsieh, Y. Hsia, T.H. Wang, C. Hsueh, C.F. Kuo, C.Y. Yeh, Successful Identification of

Nasopharyngeal Carcinoma in Nasopharyngeal Biopsies Using Deep Learning, *Cancers (Basel)*, 12 (2020).

- [33] L. Zhang, X. Wu, J. Liu, B. Zhang, X. Mo, Q. Chen, J. Fang, F. Wang, M. Li, Z. Chen, S. Liu, L. Chen, J. You, Z. Jin, B. Tang, D. Dong, S. Zhang, MRI-Based Deep-Learning Model for Distant Metastasis-Free Survival in Locoregionally Advanced Nasopharyngeal Carcinoma, *J Magn Reson Imaging*, (2020).
- [34] B. Jing, Y. Deng, T. Zhang, D. Hou, B. Li, M. Qiang, K. Liu, L. Ke, T. Li, Y. Sun, X. Lv, C. Li, Deep learning for risk prediction in patients with nasopharyngeal carcinoma using multi-parametric MRIs, *Comput Methods Programs Biomed*, 197 (2020) 105684.
- [35] C. Parmar, P. Grossmann, J. Bussink, P. Lambin, H. Aerts, Machine Learning methods for Quantitative Radiomic Biomarkers, *Sci Rep*, 5 (2015) 13087.
- [36] W. Mu, L. Jiang, J. Zhang, Y. Shi, J.E. Gray, I. Tunali, C. Gao, Y. Sun, J. Tian, X. Zhao, X. Sun, R.J. Gillies, M.B. Schabath, Non-invasive decision support for NSCLC treatment using PET/CT radiomics, *Nat Commun*, 11 (2020) 5228.
- [37] E.A. Eisenhauer, P. Therasse, J. Bogaerts, L.H. Schwartz, D. Sargent, R. Ford, J. Dancey, S. Arbuck, S. Gwyther, M. Mooney, L. Rubinstein, L. Shankar, L. Dodd, R. Kaplan, D. Lacombe, J. Verweij, New response evaluation criteria in solid tumours: revised RECIST guideline (version 1.1), *Eur J Cancer*, 45 (2009) 228-247.
- [38] P.A. Yushkevich, J. Piven, H.C. Hazlett, R.G. Smith, S. Ho, J.C. Gee, G. Gerig, User-guided 3D active contour segmentation of anatomical structures: significantly improved efficiency and reliability, *Neuroimage*, 31 (2006) 1116-1128.
- [39] J.J.M. van Griethuysen, A. Fedorov, C. Parmar, A. Hosny, N. Aucoin, V. Narayan, R.G.H. Beets-Tan, J.C. Fillion-Robin, S. Pieper, H. Aerts, Computational Radiomics System to Decode the Radiographic Phenotype, *Cancer Res*, 77 (2017) e104-e107.
- [40] H.J. Aerts, The Potential of Radiomic-Based Phenotyping in Precision Medicine: A Review, *JAMA Oncol*, 2 (2016) 1636-1642.
- [41] H. Kondo, C.D.H. Ratcliffe, S. Hooper, J. Ellis, J.I. MacRae, M. Hennequart, C.W. Dunsby, K.I. Anderson, E. Sahai, Single-cell resolved imaging reveals intra-tumor heterogeneity in glycolysis, transitions between metabolic states, and their regulatory mechanisms, *Cell Rep*, 34 (2021) 108750.